PCCP
Physical Chemistry Chemical Physics

Accepted Manuscript

This article can be cited before page numbers have been issued, to do this please use: M. Juanes, R. T. Saragi, C. Pérez, L. Enríquez, M. Jaraiz and A. Lesarri, *Phys. Chem. Chem. Phys.*, 2022, DOI: 10.1039/D2CP00479H.

View Article Online
DOI: 10.1039/D2CP00479H

ARTICLE

Torsional Chirality and Molecular Recognition: The Homo and Heterochiral Dimers of Thenyl and Furfuryl Alcohol

Received 28th January 2022,
Accepted 00th January 2022

DOI: 10.1039/x0xx00000x

Marcos Juanes,[a] Rizalina Tama Saragi,[a] Cristóbal Pérez,*[a] Lourdes Enríquez,[b] Martín Jaraíz,[b] Alberto Lesarri*[a]

Furfuryl alcohol and thenyl alcohol contain a labile torsional chiral center, producing transiently chiral enantiomers interconverting in the nanosecond time-scale. We explored chiral molecular recognition using the weakly-bound intermolecular dimers of both alcohols, freezing stereomutation. Supersonic jet broadband microwave spectroscopy revealed homo and heterochiral diastereoisomers for each alcohol dimer and the structural characteristics of the clusters. All dimers are primarily stabilized by a moderately intense O-H···O hydrogen bond, but differ in the secondary interactions, which introduce additional hydrogen bonds either to the ring oxygen in furfuryl alcohol or to the π ring system in thenyl alcohol. Density-functional calculations (B2PLYP-D3(BJ)/def2-TZVP) show no clear preferences for a particular stereochemistry in the dimers, with relative energies of the order 1-2 kJ mol^{-1}. The study suggests opportunities for the investigation of chiral recognition in molecules with torsional barriers in between transient and permanent interconversion regimes.

Introduction

Chirality recognition, defined as the non-covalent chemical interactions by which a chiral molecule (receptor/host) recognizes a specific stereoisomer (substrate/guest), remains at the core of the physical mechanisms supporting life and supramolecular Chemistry. Most of the experimental information on molecular recognition originates from condensed phases.[1,2] Alternatively, gas-phase experiments offer high-resolution,[3,4] cancelation of matrix effects,[5] direct comparison with single-molecule quantum mechanical calculations[6,7] and accurate description of non-covalent forces, necessary for future extrapolation from the molecular scale to the meso- and nano-phases.[8,9]

In this context, the recognition between molecules with transient chirality offers particular interest, as it converts indistinguishable enantiomeric monomer species into resolvable diastereomeric dimers,[10–12] quenching the stereomutation barriers and revealing the magnitude of the weak multi-contact interactions associated to the asymmetric force balance in the homo and heterochiral species.[3,4] Transient chirality originates from low stereomutation barriers, like the weak torsional barriers[13] where axial enantiomers tunnel between two mirror-image conformations. This phenomenon is designated as atropisomerism[14,15] for large torsional barriers. Most of gas-phase experiments on transient chirality synchronization have been restricted to alcohols,[16–21] where torsional barriers are quite low (3.35 kJ mol^{-1} in benzyl alcohol,[22] 4.51 kJ mol^{-1} in cyclohexanol[23]), and the associated interconversion half-lifetimes lie in the nanosecond range. Additional experiments with molecules of larger torsional barriers could eventually freeze the two enantiomers within near-isolated potential wells, illustrating the evolution from transient to conventional (kinetically inert) permanent stereocenters.[24] The investigation of stereochemical lability for different stereomutation regimes thus adds molecular information on chiral recognition not restricted to conventional tetrahedral stereogenic centers.

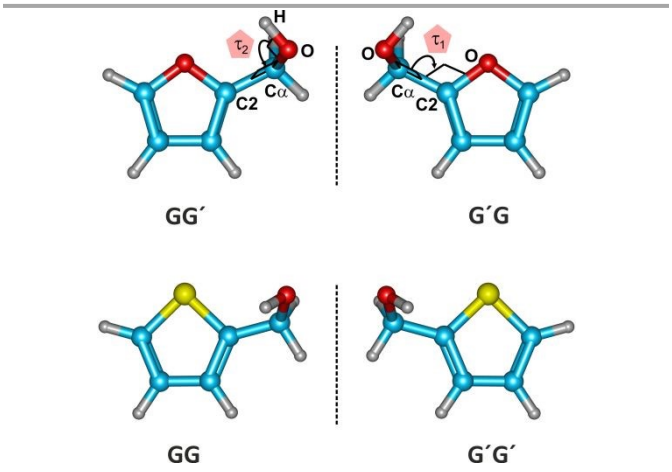

Fig. 1 Torsional enantiomers of furfuryl alcohol (upper row) and thenyl alcohol (lower row) in their most stable synclinal conformations (oxygen and sulfur atoms depicted conventionally in red and yellow, respectively).

[a] Departamento de Química Física y Química Inorgánica, Facultad de Ciencias - I.U. CINQUIMA, Universidad de Valladolid, Paseo de Belén 7, 47011 Valladolid, Spain
[b] Departamento de Electrónica, ETSIT, Universidad de Valladolid, Paseo de Belén 15, 47011 Valladolid, Spain

† Electronic Supplementary Information (ESI) available: pdf file including Figures S1-S9 and Tables S1-S16 with supporting figures, computational results and list of observed rotational transitions. See DOI: 10.1039/x0xx00000x

We report a rotational investigation on chiral recognition in the dimers of furfuryl alcohol and thenyl alcohol (Figure 1) using broadband (chirped-pulsed) microwave spectroscopy[25] and density-functional theory (DFT) calculations. The molecules present a common hydroxymethyl skeleton but different heteroatoms in the five-membered aromatic ring, designed to compare the hydrogen bond differences between sulfur and oxygen centers. Competing binding sites for dimerization and hydrogen bonding are available at the amphiprotic hydroxymethyl sidechain, the aromatic π system and the two heteroatoms.

Experimental and computational methods

The investigation of the dimers of furfuryl alcohol (2-furanmethanol, >98% GC, b.p. ~170°C) and thenyl alcohol (2-thiophenemethanol, >98% GC, b.p. ~207°C) used commercial samples and required no further purification. Both molecules were prepared as a supersonic jet using thermal vaporization. Following heating at temperatures of 85°C and 75°C, respectively, a solenoid valve (Parker, Series 9) and a pin-hole conical nozzle (0.8 mm diameter) were used to create the pulsed expansion with neon as carrier gas and backing pressures of 0.25 MPa. The typical gas pulses entering the expansion chamber had a duration of 900 μs. The expanding jet was probed with a broadband chirped-pulsed Fourier transform microwave (CP-FTMW) spectrometer[26–28] working in the 2-8 GHz frequency region. The spectrometer was based in a direct-digital design,[29] using an arbitrary waveform generator as radiation source. A sequence of five chirped-pulses of 4 μs, amplified to 20 W, excited the full 6 GHz bandwidth in each experimental event, creating a macroscopic polarization by a fast-passage mechanism.[30] The molecular emission from rotational decoherence or free-induction decay, was amplified and recorded in the time domain for about 40 μs per excitation pulse with a digital oscilloscope (20 MSamples/s). The frequency-domain spectrum was obtained with a Fourier transformation and a Kaiser-Bessel window, which produce FWHM linewidths of ca. 100 kHz. For both molecules 1 M averages were recorded at a repetition rate of 5 Hz. The uncertainty of the frequency measurements is better than 20 kHz.

Computational methods primarily used molecular orbital calculations. An initial dataset of plausible dimer structures was generated with an hybrid Monte Carlo/low-mode[31] conformational search based on molecular mechanics (MMFFs[32]). In a later stage Grimme's conformer–rotamer ensemble sampling tool (CREST[33]) was used to search for additional structures. Additional chemically reasonable structures were added manually. All starting geometries were then fully reoptimized using density-functional theory (DFT) and ab initio methods. Following different tests, we are reporting exclusively the results with the B3LYP[34] hybrid and B2PLYP[35] double-hybrid methods and D3[36] empirical dispersion terms (Becke-Johnson damping function[36]), which provided better agreement with the experiment. A polarized triple-ζ Ahlrichs' basis set def2-TZVP[37] was used in all cases, as implemented in Gaussian 16[38] and ORCA.[39] The vibrational frequency calculations used the harmonic approximation at the same level of theory. Basis set superposition errors (BSSE) in the complexation energies used the counterpoise approximation.[40] The energy decomposition used symmetry adapted perturbation theory (SAPT[41]), implemented in PSI4.[42] Finally, the analysis of non-covalent interactions used a reduced gradient of the electronic density, included in NCIPlot.[43,44]

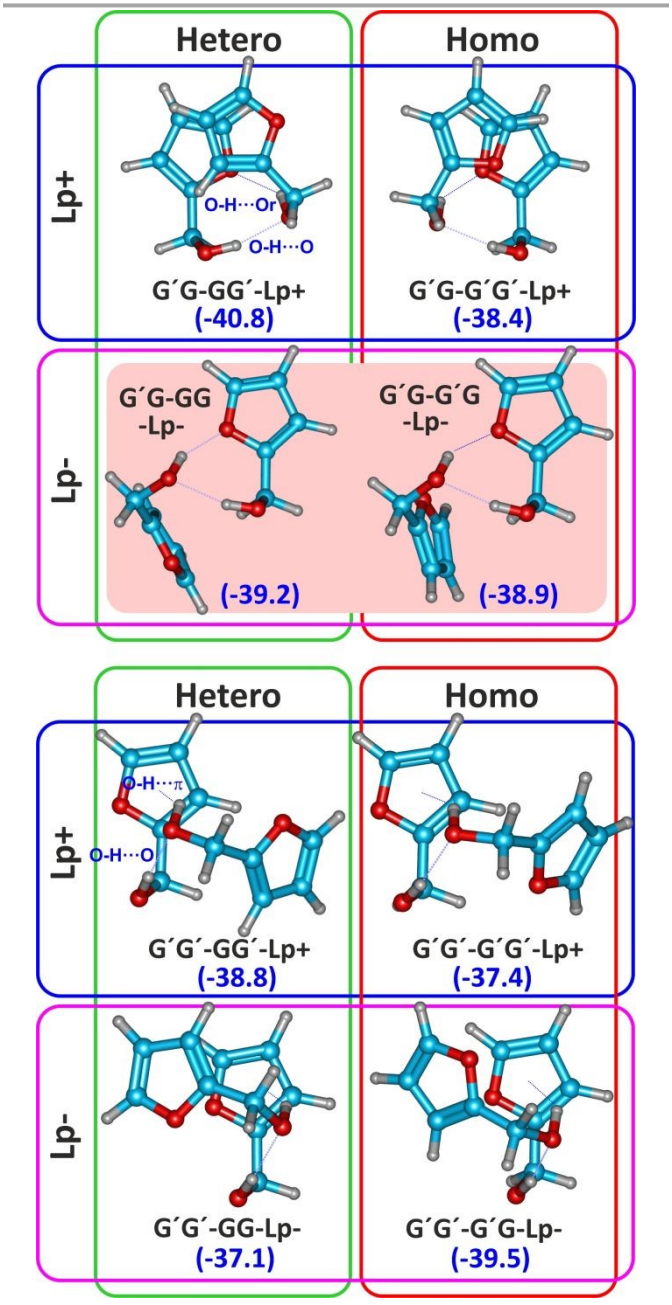

Fig. 2 Conformational search for the furfuryl alcohol dimer (complexation energies in parentheses, B2PLYP/def2-TZVP, see Table 1), highlighting the two observed isomers. The most stable isomer families differ in the aggregation pattern, either O-H···O-H···O_r (upper panel) or O-H···O-H···π

Results and discussion

Potential energy surface

The bidimensional potential energy surface of the monomers is characterized by two dihedrals defining the elevation and position of the alcohol group (τ_1(OCα-C2O/S) and τ_2(HO-CαC2) in Figure 1).[45–47] Both molecules share a synclinal (*gauche*) sidechain orientation (τ_1 ~ ±60-70°, denoted G or G´ attending to the torsion sign), but differ in the orientation of the terminal alcohol hydrogen atom, either forming O-H···O (τ_2 ~ ∓58° or GG´) or O-H···π intramolecular interactions (τ_2 ~ ±50° or GG). Reflection through the ring plane produces the enantiomeric conformations of Figure 1 (GG´ ≡ G´G, etc) and Tables S1-S2 (ESI†).

The torsional barriers between enantiomers were calculated as 14-17 kJ mol^{-1} (B3LYP-D3(BJ)) in Figures S1-S2 (ESI†), i.e., a factor of 2-3 larger than the alcohol torsions. These stereomutation barriers, despite still categorized as rapidly equilibrating mixtures (Class I: < 80 kJ mol^{-1}) by LaPlante,[48] make both systems interesting to examine possible torsional deformations on complexation, the preferences for homo- or heterochiral aggregation and the magnitude of the chirodiastaltic energies.[49–51] At the same time, the comparison between the non-covalent interactions from the sulfur and oxygen atoms in the furanyl and thenyl groups adds empirical information on sulfur hydrogen bonds, scarcely investigated.[52–55] Higher-energy conformations (Tables S3-S4, ESI†) are expected to be depopulated in a jet expansion.[46,47]

Torsional enantiomerism anticipated the formation of homochiral or heterochiral dimers for each molecule. Two enantiomers with identical spectroscopic properties would then be expected (i.e., homo GG´-GG´ = G´G-G´G and heterochiral GG´-G´G = G´G-GG´ furfuryl alcohol dimers, proton donor denoted first). However, unlike in permanent stereocenters, the torsional adaptability of the sidechain may render additional stereoisomers feasible for the dimers. In particular, isomers with anticlinal (A) orientations of the side chain were predicted in the computations, competing with the synclinal conformations. Moreover, the presence of two diastereotopic acceptor lone pairs (denoted Lp+/- according to the dihedral LpO-CαC2) and the multiple possibilities for interaction between the polar alcohol groups and the two ring molecules further complicate the conformational space and suggest a shallow potential energy surface.

The results of a (B3LYP-D3(BJ)) density-functional theory conformational search for the furfuryl alcohol dimer are collected in Figure 2 and Table S5 (ESI†). The most stable geometries exhibit hinged geometries which swing the two rings around a primary O-H···O hydrogen bond axis. The alcohol group in the proton acceptor then establishes a second cooperative O-H···O$_r$ hydrogen bond to the donor ring oxygen (O$_r$), closing a seven membered-ring. Additional C(sp^3)-H···π interactions finally determine the tilting between the two rings. Because both homo/heterochiral and Lp+/- geometries are feasible, four low-lying (< 4 kJ mol^{-1}) isomers may be conceived for this particular geometry, with the two monomers respecting the preferred synclinal (G) sidechain.

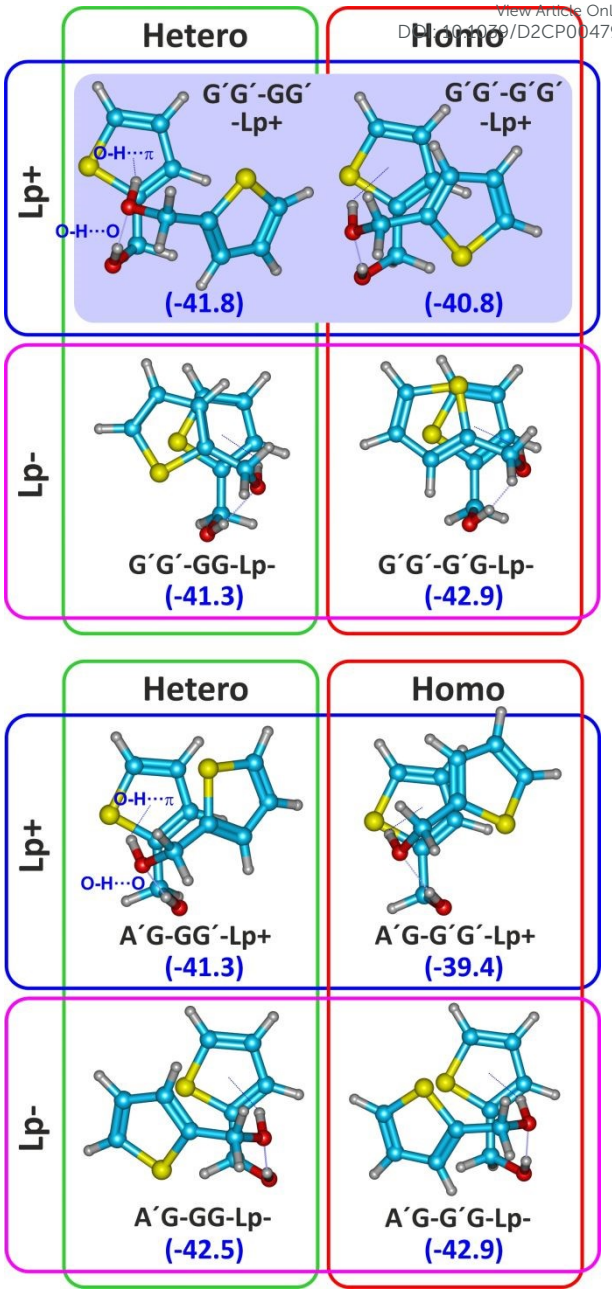

Fig. 3 Conformational search for the thenyl alcohol dimer (complexation energies in parentheses, B2PLYP/def2-TZVP, see Table 2), highlighting the two observed isomers (in blue). The most stable isomer families share the O-H···O-H···π aggregation pattern, but differ in the use of synclinal (G, upper panel) or anti (A, lower panel) monomers.

A second structural family in Figure 2 present also a hinged O-H···O hydrogen bond but complemented with a second O-H···π hydrogen bond to the opposite ring. These interactions may be supplemented by weak C(sp^2)-H···π contacts between the two rings and similarly offer four alternative homo-/heterochiral and Lp+/Lp- geometries. Other structures sharing the O-H···O hydrogen bond and a different anticlinal sidechain in the proton donor are illustrated in Figure S3 (ESI†). Interestingly, no stacking or symmetric structures were observed for low-lying isomers. The first (C_i) symmetric

View Article Online
DOI: 10.1039/D2CP00479H

Table 1 Rotational parameters for the dimer of furfuryl alcohol.

	Experiment		Theory	
	Isomer 1	Isomer 2	Homochiral	Heterochiral
			G´G-G´G-Lp-	G´G-GG-Lp-
A / MHz [a]	1054.71641(47) [d]	1096.59893(71)	1055.02	1096.27
B / MHz	436.11244(22)	414.49672(44)	443.70	421.88
C / MHz	419.35674(23)	400.89791(55)	427.77	409.86
D_J / kHz	0.2218(14)	0.1640(33)	0.198	0.159
D_{JK} / kHz	-0.7835(41)	-0.6516(78)	-0.676	-0.667
D_K / kHz	1.586(10)	1.749(26)	1.461	1.692
d_1 / kHz	0.03884(46)	0.0162(13)	-0.029	0.018
d_2 / kHz	[0.] [e]	-0.00155(25)	0.002	-0.002
$\|\mu_a\|$ / D	++	-	0.9	0.1
$\|\mu_b\|$ / D	+++	-	2.6	0.3
$\|\mu_c\|$ / D	++	++	1.3	3.8
N [b]	202	87		
σ / kHz	12.6	13.1		
ΔE / kJ mol^{-1} [c]			0.7	2.2
ΔG /kJ mol^{-1}			0.1	2.1
ΔE_C / kJ mol^{-1}			-38.9	-39.2

[a]Rotational constants (A, B, C), Watson's S-reduction centrifugal distortion constants (D_J, D_{JK}, D_K, d_1, d_2) and electric dipole moments (μ_α, α = a, b, c). [b]Number of measured transitions (N) and standard deviation of the fit (σ). [c]Relative energies corrected with the zero-point energy (ΔE), Gibbs energy (ΔG, 298K, 1 atm) and complexation energy (including BSSE corrections) using B2PLYP-D3(BJ) and the basis set def2-TZVP (ΔE_c). [d]Standard errors in parentheses in units of the last digit. [e]Value fixed to zero.

structure in Figure S4 (ESI†) has an electronic energy of ca. 9 kJ mol^{-1}. Once the main conformation preferences were stablished, additional B2PLYP-D3(BJ) reoptimizations were completed for the low-lying isomers in Table S6 (ESI†).

For the thenyl mercaptan dimer the geometry optimization showed a larger dependence on the computational method and convergence criteria. Three main structural patterns were detected for the thenyl dimers, characterized by the absence of any O-H···S hydrogen bond involving the alcohol and the ring heteroatom. For this reason, the counterparts of the four most stable species of (furfuryl alcohol)$_2$ were not found here. On the other hand, the preferred thenyl dimers in Figure 3 and Table S7 (ESI†), showed resemblance with the second family of furfuryl aggregates, presenting hinged tilted geometries based in the primary O-H···O hydrogen bond axis, together with secondary O-H···π alcohol interactions to the π ring. This motif offers four homo/heterochiral and Lp+/- variations, with the two monomers in the preferred synclinal (G) sidechain. Additional geometries in which the donor hydrogen bond adopts an anticlinal orientation on complexation were also predicted, for which other four (homo/heterochiral and Lp+/-) geometries in Figure 3 are conceivable. Alternative parallel-displaced stacking geometries were predicted at relatively small energies (>2-4 kJ mol^{-1}, Figure S5, ESI†), either with synclinal-synclinal or synclinal-anticlinal orientations. The only low-energy symmetric dimer presented a C_2 point group (Figure S6, ESI†) and electronic energies of ca. 5 kJ mol^{-1}. The low-lying geometries were reoptimized with B2PLYP in Table S8 (ESI†).

Rotational spectrum

The computational predictions were assessed against the jet-cooled microwave spectrum (see Experimental Methods). The search for the dimers, illustrated in Figures S7-S8 (ESI†), finally led to the assignment of two isomers for the dimers of furfuryl

Table 2 Rotational parameters for the dimer of thenyl alcohol.

	Experiment		Theory	
	Isomer 1	Isomer 2	Heterochiral	Homochiral
			G´G´-GG´-Lp+	G´G´-G´G´-Lp+
A / MHz [a]	824.07911(75)	813.40958(30)	859.03	829.55
B / MHz	382.68442(25)	394.62969(16)	358.74	393.18
C / MHz	348.11932(24)	354.53843(17)	329.32	357.42
D_J / kHz	0.1066(11)	0.16796(66)	0.517	0.241
D_{JK} / kHz	-0.1297(46)	-0.4034(19)	1.312	-0.712
D_K / kHz	0.272(34)	0.5508(32)	-1.612	0.912
d_1 / kHz	-0.00658(77)	-0.01353(29)	-0.128	-0.045
d_2 / kHz	[0.0] [b]	0.0	-0.005	-0.003
$\|\mu_a\|$ / D	++	++	2.1	2.1
$\|\mu_b\|$ / D	++	+++	2.6	3.7
$\|\mu_c\|$ / D	-	-	0.4	0.1
N	138	266		
σ / kHz	10.3	12.5		
ΔE / kJ mol^{-1}			1.6	0.4
ΔG /kJ mol^{-1}			0.0	1.1
ΔE_C / kJ mol^{-1}			-41.8	-40.8

[a]Parameter definition as in Table 1. [b]Parameters in square brackets fixed to zero.

alcohol and furfuryl mercaptan. In all cases the spectrum was reproduced to experimental accuracy with a semi-rigid rotor Hamiltonian,[56] and no large-amplitude motions or tunnelling effects were observed. The final spectroscopic parameters are shown in Tables 1 and 2, while the measured rotational transitions are collected in Tables S9-S12 (ESI†).

Noticeably, the two isomers of each dimer showed very similar rotational constants (i.e, a difference below 12 MHz for thenyl mercaptan or 42 MHz for furfuryl alcohol). This fact suggested close molecular geometries for the two species of each dimer, probably sharing the most important structural characteristics. A comparison of the rotational constants with the computations then assured the conformational assignment. For the furfuryl alcohol dimers the two homo and heterochiral isomers in Figure 2 were readily assigned, differing only in the chirality of the proton acceptor (G´G-GG-Lp- and G´G-G´G-Lp-). In both cases the agreement between predictions and experiment in Table 1 was very satisfactory (<2.2 %). However, for the thenyl alcohol dimer the situation was more difficult. Initially, only a single heterochiral isomer (G´G´-GG´-Lp+) in Figure 3 could be assigned, and the second experimental partner could not be matched with any of the B3LYP-D3(BJ) predictions of Table S7 (ESI†). This fact motivated new computations with MN-15L, B2PLYP-D3(BJ) and MP2, which converged to close structural minima of the homochiral form with better agreement with the experiment. Based on this fact, the second experimental isomer was assigned to the homochiral counterpart G´G´-G´G´-Lp+. The relative deviation of the B2PLYP predictions in Table 2 remained below 0.4-2.0% for the heterochiral dimer but was worse for the homochiral form (4.2-6.3%). No other species of reasonable intensity could be found in the spectrum.

Non-covalent interactions

The non-covalent interactions stabilizing the two alcohol dimers were analysed structurally, energetically and using the electronic density topology.[44] The leading interaction for the furfuryl dimer structures (Tables S13-S16, ESI†) is the shorter and relatively linear O-H···O hydrogen bond, slightly larger in the heterochiral dimer (B2PLYP: r(O-H···O) = 1.982 Å, ∠(O-H···O) = 158.6°) than in the homochiral form (r(O-H···O) = 1.938 Å, ∠(O-H···O) = 161.8°). This interaction bears similarities with the water monohydrates.[46,47] A second cooperative O-H···O_r hydrogen bond to the ring oxygen closes a cyclic structure, also observed in the monohydrates. This hydrogen bond shows larger contacts for the homochiral (B2PLYP: r(O-H···O_r) = 2.015 Å, ∠(O-H···O_r) = 148.8°) than for the heterochiral isomer (r(O-H···O_r) = 1.974 Å, ∠(O-H···O_r) = 156.0°). In the thenyl dimers the primary O-H···O hydrogen bond is also locking the two alcohol groups, now slightly shorter in the heterochiral (B2PLYP: r(O-H···O_r) = 1.919 Å, ∠(O-H···O_r) = 166.4°) than in the homochiral form (r(O-H···O_r) = 1.991 Å, ∠(O-H···O_r) = 163.5°). This interaction again parallels the observation in the thenyl monohydrate (B2PLYP: r(O-H···O_r) = 1.965 Å, ∠(O-H···O_r) = 159.6°), where, characteristically, the secondary hydrogen bond targets the π system. Non-covalent interactions in the four observed dimers are compared in Figure 4 using Johnson-Contreras's reduced electronic density mapping,[57] identifying the hydrogen bonds and other weakly attractive regions around the two rings.

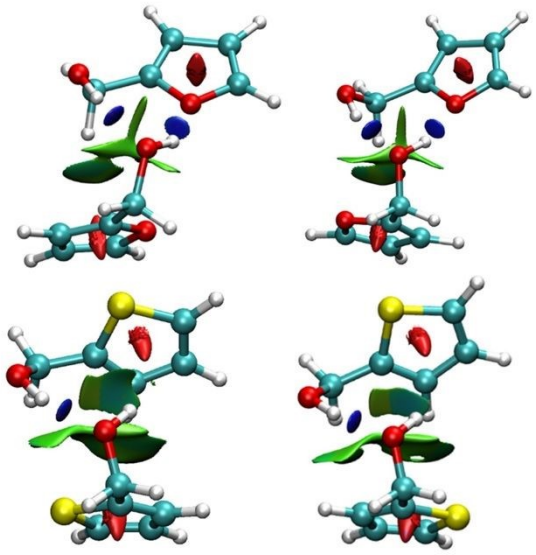

Fig. 4 NCI plots for the homodimers of furfuryl alcohol (upper row) compared to thenyl alcohol (lower row), mapping non-covalent interaction (isosurfaces of $s(r)$=0.5 a.u., colored by sign $(\lambda_2) \times \rho(r)$, see refs. 43-44). The blue shades indicate attractive interactions (associated to bond critical points), green colors indicate weak interactions and red represents repulsive interactions (like the ring critical points).

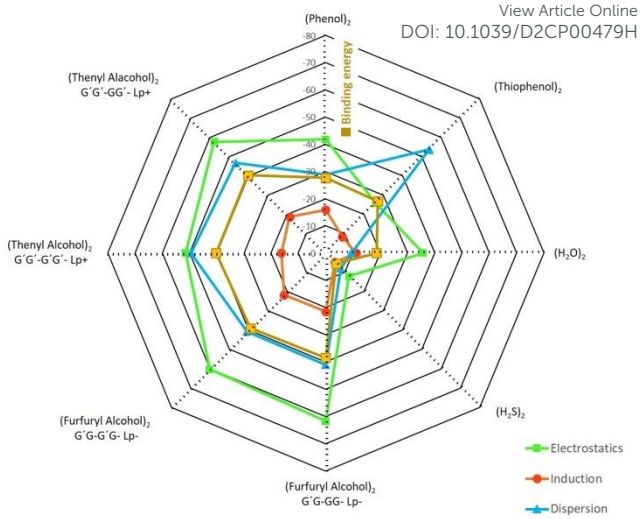

Fig. 5 A radar chart showing the SAPT2+(3) binding energy decomposition for the furfuryl alcohol and thenyl alcohol dimers (kJ mol^{-1}), comparing the attractive energetic contributions to those of the related dimers reported in Table S17 (ESI).

The predictions for the complexation energies of the alcohol dimers are quite similar, slightly larger for the thenyl alcohol dimer (B2PLYP: -41.8 and -40.8 kJ mol^{-1}) compared to the furfuryl aggregate (-38.9 and -39.2 kJ mol^{-1}). These calculations would emphasize the leading stabilizer role of the primary O-H···O hydrogen bond, but they contrast with the stability of the monohydrates, where the furfuryl compound has larger complexation energies. The B3LYP-D3(BJ) complexation energies are generally 3-5 kJ mol^{-1} larger than the B2PLYP-D3(BJ) values.

The participation of electrostatic and dispersion forces in the dimer stability has been estimated using SAPT2+(3) energy decomposition. The calculations in Figure 5 and Table S17 (ESI†) suggest a dominant electrostatic character for the two alcohols, i.e., 49-50% and 44-47% of the total attractive energy, respectively, for the furfuryl and thenyl dimers, slightly smaller than in the monohydrates (56-57%). At the same time, the dimers show a considerable increase of the dispersion contributions, associated to the two aromatic rings (33% and 38-42% for the furfuryl and thenyl dimers, respectively vs. 22-25% in the monohydrates). Calculations on related alcohols[18,57,58] and thiols,[53,54] and the dispersive pyridine-methane dimer[59] are included for comparison.

Conclusion

The experimental observation of homochiral and heterochiral isomers for the two alcohols represents a rare occasion where different torsional isomers have been observed independently. The close relative energies, even predicted at B2PLYP-D3(BJ) level, were inconclusive on the identification of the global minima, and relied on the experimental findings. The two alcohol dimers were predicted with opposing stereochemical preferences (homochiral for the furfuryl dimer, heterochiral for the thenyl dimer) but the small chirodiastaltic energies of 1-2 kJ mol^{-1} prevent any generalization on the dimerization properties and aggregation preferences. Considering the small interconversion barriers between the torsional isomers new experiments can be designed to explore the transition between torsional labile compounds and permanent stereocenters on molecular aggregation.

This study also provides an accurate description of the intermolecular forces in the dimerization process, characterized by a cooperative behavior of two hydrogen bonds including interactions to the ring heteroatom or the π ring.[46,47,55,60] Furthermore, the comparison between the furfuryl and thenyl compounds explores the different role of the hydrogen bond involving sulfur, which in the thenyl compounds have less priority that the interaction to the π ring system. The molecular description of the two alcohol dimers, while structurally similar to the monohydrates, offers a completely different combination of dispersion effects, calling for adequate dispersion-corrected quantum mechanical models. In this sense we have found interesting issues associated to the structural convergence in the two DFT methods used, emphasizing the importance of the functional selection, calculation grid, convergence thresholds and other numerical problems. Finally, the role of gas-phase intermolecular clusters as interaction models for molecular aggregation should be stressed, outlining the important collaboration between rotationally resolved experiments and DFT and ab initio methods.

Author Contributions

View Article Online
DOI: 10.1039/D2CP00479H

Conceptualization, C.P. and A.L.; methodology, C.P. and A.L.; software, L.E. and M.J..; validation, M.J. and R.T.S.; formal analysis, M.J.; investigation, M.J. and R.T.S.; resources, A.L.; data curation, A.L.; writing—original draft preparation, A.L.; writing—review and editing, R.T.S., M.J., C.P., L.E. and M.J.; visualization, M.J.; supervision, A.L.; project administration, C.P. and A.L.; funding acquisition, A.L.

Conflicts of interest

There are no conflicts to declare.

Acknowledgements

Funding support from the Spanish MICINN-FEDER (grant PGC2018-098561-B-C22) is gratefully acknowledged. M.J. and R.T.S. are thankful for predoctoral contracts from the MICINN and UVa, respectively.

References

1 K. Ariga, H. Ito, J. P. Hill and H. Tsukube, Molecular recognition: From solution science to nano/materials technology, *Chem. Soc. Rev.*, 2012, **41**, 5800–5835.

2 E. Persch, O. Dumele and F. Diederich, Molecular recognition in chemical and biological systems, *Angew. Chemie - Int. Ed.*, 2015, **54**, 3290–3327.

3 A. Zehnacker and M. A. Suhm, Chirality Recognition between Neutral Molecules in the Gas Phase, *Angew. Chemie Int. Ed.*, 2008, **47**, 6970–6992.

4 A. Zehnacker, Ed., *Chiral Recognition in the Gas Phase*, CRC Press, Boca Raton, Florida, 2010.

5 J.-P. Schermann, *Spectroscopy and Modeling of Biomolecular Building Blocks*, Elsevier, 2008.

6 P. Hobza and K. Muller-Dethlefs, *Non-Covalent Interactions*, Royal Society of Chemistry, Cambridge, 2009.

7 S. Scheiner, Ed., *Noncovalent Forces*, Springer International Publishing, Cham, Switzerland, 2015, vol. 19.

8 M. Liu, L. Zhang and T. Wang, Supramolecular chirality in self-Assembled systems, *Chem. Rev.*, 2015, **115**, 7304–7397.

9 J. R. Brandt, F. Salerno and M. J. Fuchter, The added value of small-molecule chirality in technological applications, *Nat. Rev. Chem.*, , DOI:10.1038/s41570-017-0045.

10 M. Pierini, A. Troiani, M. Speranza, S. Piccirillo, C. Bosman, D. Toja and A. Giardini-Guidoni, Gas-Phase Enantiodifferentiation of Chiral Molecules: Chiral Recognition of 1-Phenyl-1-propanol/2-Butanol Clusters by Resonance Enhanced Multiphoton Ionization Spectroscopy, *Angew. Chemie - Int. Ed.*, 1997, **36**, 1729–1731.

11 K. Le Barbu, V. Brenner, P. Millié, F. Lahmani and A. Zehnacker-Rentien, An Experimental and Theoretical Study of Jet-Cooled Complexes of Chiral Molecules: The Role of Dispersive Forces in Chiral Discrimination, *J. Phys. Chem. A*, 1998, **102**, 128–137.

12 N. Borho, T. Häber and M. A. Suhm, Chiral self-recognition in the gas phase: the case of glycidol dimers, *Phys. Chem. Chem. Phys.*, 2001, **3**, 1945–1948.

13 N. A. Seifert, C. Pérez, J. L. Neill, B. H. Pate, M. Vallejo-López, A. Lesarri, E. J. Cocinero and F. Castaño, Chiral recognition and atropisomerism in the sevoflurane dimer, *Phys. Chem. Chem. Phys.*, 2015, **17**, 18282–18287.

14 M. Oki, in *Topics in Stereochemistry, vol. 14*, ed. S. H. Allinger, Norman L.;Eliel, Ernest L.;Wilen, John Wiley & Sons, Inc, New York, NY, 1983, pp. 1–82.

15 P. Ottaviani, A. Maris and W. Caminati, Atropisomerism in bisphenols: Free jet absorption millimeter wave study of 2,2'-biphenol, *J. Mol. Struct.*, 2004, **695–696**, 353–356.

16 M. S. Snow, B. J. Howard, L. Evangelisti and W. Caminati, From Transient to Induced Permanent Chirality in 2-Propanol upon Dimerization: A Rotational Study, *J. Phys. Chem. A*, 2011, **115**, 47–51.

17 A. Maris, B. M. Giuliano, D. Bonazzi and W. Caminati, Molecular recognition of chiral conformers: A rotational study of the dimers of glycidol, *J. Am. Chem. Soc.*, 2008, **130**, 13860–13861.

18 M. Juanes, I. Usabiaga, I. León, L. Evangelisti, J. A. Fernández and A. Lesarri, The Six Isomers of the Cyclohexanol Dimer: A Delicate Test for Dispersion Models, *Angew. Chemie Int. Ed.*, 2020, **59**, anie.202005063.

19 X. Liu, N. Borho and Y. Xu, Molecular self-recognition: Rotational spectra of the dimeric 2-fluoroethanol conformers, *Chem. - A Eur. J.*, 2009, **15**, 270–277.

20 J. Thomas and Y. Xu, Chirality synchronization in trifluoroethanol dimer revisited: The missing heterochiral dimer, *J. Phys. Chem. Lett.*, 2014, **5**, 1850–1855.

21 S. Oswald, N. A. Seifert, F. Bohle, M. Gawrilow, S. Grimme, W. Jäger, Y. Xu and M. A. Suhm, The Chiral Trimer and a Metastable Chiral Dimer of Achiral Hexafluoroisopropanol: A Multi-Messenger Study, *Angew. Chemie - Int. Ed.*, 2019, **58**, 5080–5084.

22 K. A. Utzat, R. K. Bohn, J. A. Montgomery, H. H. Michels and W. Caminati, Rotational spectrum, tunneling motions, and potential barriers of benzyl alcohol, *J. Phys. Chem. A*, 2010, **114**, 6913–6916.

23 M. Juanes, W. Li, L. Spada, L. Evangelisti, A. Lesarri and W. Caminati, Internal dynamics of cyclohexanol and the cyclohexanol-water adduct, *Phys. Chem. Chem. Phys.*, 2019, **21**, 3676–3682.

24 C. Pérez, A. L. Steber, A. Krin and M. Schnell, State-Specific Enrichment of Chiral Conformers with Microwave Spectroscopy, *J. Phys. Chem. Lett.*, 2018, **9**, 4539–4543.

25 G. B. Park and R. W. Field, Perspective: The first ten years of broadband chirped pulse Fourier transform microwave spectroscopy, *J. Chem. Phys.*, 2016, **144**, 1–10.

26 S. T. Shipman and B. H. Pate, in *Handbook of High-resolution Spectroscopy*, eds. F. Merkt and M. Quack, John Wiley & Sons, Ltd, New York, 2011, pp. 801–828.

27 J.-U. Grabow, in *Handbook of High-resolution Spectroscopy*, eds. F. Merkt and M. Quack, John Wiley & Sons, Ltd, New York, 2011, pp. 723–799.

28 W. Caminati and J.-U. Grabow, in *Frontiers and Advances in Molecular Spectroscopy*, ed. J. Laane, Elsevier Inc., 2018, pp. 569–598.

29 J. L. Neill, S. T. Shipman, L. Alvarez-Valtierra, A. Lesarri, Z. Kisiel and B. H. Pate, Rotational spectroscopy of iodobenzene and iodobenzene-neon with a direct digital 2-8 GHz chirped-pulse Fourier transform microwave spectrometer, *J. Mol. Spectrosc.*, 2011, **269**, 21–29.

30 J. C. McGurk, T. G. Schmalz and W. H. Flygare, Fast passage in

rotational spectroscopy: Theory and experiment, *J. Chem. Phys.*, 1974, **60**, 4181–4188.

31 G. M. Keserû and I. Kolossváry, Fully Flexible Low-Mode Docking: Application to Induced Fit in HIV Integrase, *J. Am. Chem. Soc.*, 2001, **123**, 12708–12709.

32 T. A. Halgren, MMFF VI. MMFF94s option for energy minimization studies, *J. Comput. Chem.*, 1999, **20**, 720–729.

33 P. Pracht, F. Bohle and S. Grimme, Automated exploration of the low-energy chemical space with fast quantum chemical methods, *Phys. Chem. Chem. Phys.*, 2020, **22**, 7169–7192.

34 A. D. Becke, Density-functional thermochemistry. III. The role of exact exchange, *J. Chem. Phys.*, 1993, **98**, 5648–5652.

35 S. Grimme and F. Neese, Double-hybrid density functional theory for excited electronic states of molecules, *J. Chem. Phys.*, 2007, **127**, 1–18.

36 S. Grimme, S. Ehrlich and L. Goerigk, Effect of the damping function in dispersion corrected density functional theory, *J. Comput. Chem.*, 2011, **32**, 1456–1465.

37 F. Weigend and R. Ahlrichs, Balanced basis sets of split valence, triple zeta valence and quadruple zeta valence quality for H to Rn: Design and assessment of accuracy, *Phys. Chem. Chem. Phys.*, 2005, **7**, 3297.

38 M. J. Frisch, G. W. Trucks, H. B. Schlegel, G. E. Scuseria, M. A. Robb, J. R. Cheeseman, G. Scalmani, V. Barone, G. A. Petersson, H. Nakatsuji, X. Li, M. Caricato, A. V. Marenich, J. Bloino, B. G. Janesko, R. Gomperts, B. Mennucci, H. P. Hratchian, J. V. Ortiz, A. F. Izmaylov, J. L. Sonnenberg, Williams, F. Ding, F. Lipparini, F. Egidi, J. Goings, B. Peng, A. Petrone, T. Henderson, D. Ranasinghe, V. G. Zakrzewski, J. Gao, N. Rega, G. Zheng, W. Liang, M. Hada, M. Ehara, K. Toyota, R. Fukuda, J. Hasegawa, M. Ishida, T. Nakajima, Y. Honda, O. Kitao, H. Nakai, T. Vreven, K. Throssell, J. A. Montgomery Jr., J. E. Peralta, F. Ogliaro, M. J. Bearpark, J. J. Heyd, E. N. Brothers, K. N. Kudin, V. N. Staroverov, T. A. Keith, R. Kobayashi, J. Normand, K. Raghavachari, A. P. Rendell, J. C. Burant, S. S. Iyengar, J. Tomasi, M. Cossi, J. M. Millam, M. Klene, C. Adamo, R. Cammi, J. W. Ochterski, R. L. Martin, K. Morokuma, O. Farkas, J. B. Foresman and D. J. Fox, 2016.

39 F. Neese, Software Update: the ORCA Program System, version 4.0, *WIREs Comput. Mol. Sci.*, 2018, **8**, 1.

40 S. F. Boys and F. Bernardi, The calculation of small molecular interactions by the differences of separate total energies. Some procedures with reduced errors, *Mol. Phys.*, 1970, **19**, 553–566.

41 B. Jeziorski, R. Moszynski and K. Szalewicz, Perturbation Theory Approach to Intermolecular Potential Energy Surfaces of van der Waals Complexes, *Chem. Rev.*, 1994, **94**, 1887–1930.

42 R. M. Parrish, L. A. Burns, D. G. A. Smith, A. C. Simmonett, A. E. DePrince, E. G. Hohenstein, U. Bozkaya, A. Y. Sokolov, R. Di Remigio, R. M. Richard, J. F. Gonthier, A. M. James, H. R. McAlexander, A. Kumar, M. Saitow, X. Wang, B. P. Pritchard, P. Verma, H. F. Schaefer, K. Patkowski, R. A. King, E. F. Valeev, F. A. Evangelista, J. M. Turney, T. D. Crawford and C. D. Sherrill, Psi4 1.1: An Open-Source Electronic Structure Program Emphasizing Automation, Advanced Libraries, and Interoperability, *J. Chem. Theory Comput.*, 2017, **13**, 3185–3197.

43 E. R. Johnson, S. Keinan, P. Mori-Sánchez, J. Contreras-García, A. J. Cohen and W. Yang, Revealing noncovalent interactions, *J. Am. Chem. Soc.*, 2010, **132**, 6498–6506.

44 J. Contreras-García, E. R. Johnson, S. Keinan, R. Chaudret, J. P. Piquemal, D. N. Beratan and W. Yang, NCIPLOT: A program for plotting noncovalent interaction regions, *J. Chem. Theory Comput.*, 2011, **7**, 625–632.

45 K.-M. Marstokk, H. Møllendal, H. Stüger, H. V. Volden, D.-N. Wang, G. B. Paulsen, R. I. Nielsen, C. E. Olsen, C. Pedersen and C. E. Stidsen, Microwave Spectrum, Conformational Equilibrium and Ab Initio Calculations for 2-Furanmethanol (Furfuryl Alcohol)., *Acta Chem. Scand.*, 1994, **48**, 25–31.

46 M. Juanes, A. Lesarri, R. Pinacho, E. Charro, J. E. Rubio, L. Enríquez and M. Jaraíz, Sulfur Hydrogen Bonding in Isolated Monohydrates: Furfuryl Mercaptan versus Furfuryl Alcohol, *Chem. - A Eur. J.*, 2018, **24**, 6564–6571.

47 M. Juanes, R. T. Saragi, R. Pinacho, J. E. Rubio and A. Lesarri, Sulfur hydrogen bonding and internal dynamics in the monohydrates of thenyl mercaptan and thenyl alcohol, *Phys. Chem. Chem. Phys.*, 2020, **22**, 12412–12421.

48 S. R. Laplante, L. D. Fader, K. R. Fandrick, D. R. Fandrick, O. Hucke, R. Kemper, S. P. F. Miller and P. J. Edwards, Assessing atropisomer axial chirality in drug discovery and development, *J. Med. Chem.*, 2011, **54**, 7005–7022.

49 D. P. Craig and D. P. Mellor, in *Bonding Structure. Topics in Current Chemistry, 63*, Springer-Verlag, Berlin/Heidelberg, 1976, pp. 1–48.

50 S. Portmann, A. Inauen, H. P. Lüthi and S. Leutwyler, Chiral discrimination in hydrogen-bonded complexes, *J. Chem. Phys.*, 2000, **113**, 9577–9585.

51 I. Alkorta and J. Elguero, Discrimination of hydrogen-bonded complexes with axial chirality, *J. Chem. Phys.*, 2002, **117**, 6463–6468.

52 H. S. Biswal, S. Bhattacharyya, A. Bhattacherjee and S. Wategaonkar, Nature and strength of sulfur-centred hydrogen bonds: Laser spectroscopic investigations in the gas phase and quantum-chemical calculations, *Int. Rev. Phys. Chem.*, 2015, **34**, 99–160.

53 A. Das, P. K. Mandal, F. J. Lovas, C. Medcraft, N. R. Walker and E. Arunan, The H2S Dimer is Hydrogen-Bonded: Direct Confirmation from Microwave Spectroscopy, *Angew. Chemie Int. Ed.*, 2018, **57**, 15199–15203.

54 R. T. Saragi, M. Juanes, C. Pérez, P. Pinacho, D. S. Tikhonov, W. Caminati, M. Schnell and A. Lesarri, Switching Hydrogen Bonding to π-Stacking: The Thiophenol Dimer and Trimer, *J. Phys. Chem. Lett.*, 2021, **12**, 1367–1373.

55 R. T. Saragi, M. Juanes, R. Pinacho, J. E. Rubio, J. A. Fernández and A. Lesarri, Molecular Recognition, Transient Chirality and Sulfur Hydrogen Bonding in the Benzyl Mercaptan Dimer, *Symmetry (Basel).*, 2021, **13**, 2022.

56 J. K. G. Watson, in *Vibrational Spectra and Structure, vol. 6*, ed. J. R. Durig, Elsevier B.V., Amsterdam, 1977, pp. 1–89.

57 N. A. Seifert, A. L. Steber, J. L. Neill, C. Pérez, D. P. Zaleski, B. H. Pate and A. Lesarri, The interplay of hydrogen bonding and dispersion in phenol dimer and trimer: Structures from broadband rotational spectroscopy, *Phys. Chem. Chem. Phys.*, 2013, **15**, 11468–11477.

58 T. R. Dyke, K. M. Mack and J. S. Muenter, The structure of water dimer from molecular beam electric resonance spectroscopy, *J. Chem. Phys.*, 1977, **66**, 498–510.

59 Q. Gou, L. Spada, M. Vallejo-López, A. Lesarri, E. J. Cocinero and W.

View Article Online
DOI: 10.1039/D2CP00479H

Caminati, Interactions between alkanes and aromatic molecules: A rotational study of pyridine-methane, *Phys. Chem. Chem. Phys.*, 2014, **16**, 13041–13046.

60 R. Medel, A. Camiruaga, R. T. Saragi, P. Pinacho, C. Pérez, M. Schnell, A. Lesarri, M. A. Suhm and J. A. Fernández, Rovibronic signatures of molecular aggregation in the gas phase: subtle homochirality trends in the dimer, trimer and tetramer of benzyl alcohol, *Phys. Chem. Chem. Phys.*, 2021, **23**, 23610–23624.